

1 **Linking Weather Regimes to the Variability of Warm-Season Tornado**
2 **Activity over the United States**

3 Authors: Matthew Graber¹, Zhuo Wang¹, & Robert J. Trapp¹

4 ¹Department of Climate, Meteorology, & Atmospheric Sciences, University of Illinois Urbana-
5 Champaign, Urbana, 61820, United States

6
7 *Correspondence to: Zhuo Wang (zhuowang@illinois.edu)*

8 **Abstract**

9 The contiguous United States (CONUS) experiences considerable interannual variability in
10 tornado activity. The high impacts of tornadoes motivate the need to better understand the link
11 between seasonal tornado activity and large-scale atmospheric circulation, which may contribute
12 to better seasonal prediction. We employed K-means clustering analysis of 500 hPa geopotential
13 height (500H) daily anomalies from the ERA-5 reanalysis and identified five warm-season
14 weather regimes (WRs). Certain WRs are shown to strongly affect tornado activity, especially
15 outbreaks, due to their relationship with environmental parameters including convective
16 available potential energy (CAPE) and vertical wind shear (VWS). In particular, WR-B, which is
17 characterized by a three-cell wave-like pattern with an anomalous low over the central-CONUS,
18 is associated with enhanced CAPE and VWS in tornado-prone regions and represents a tornado-
19 favorable environment. Persistent WRs, those lasting for ≥ 5 consecutive days, are associated
20 with 76% of all tornado outbreaks (days with >10 EF-1+ tornadoes) since 1960, ~~with a~~
21 persistent WR-B ~~accounting, in particular, accounts~~ for about 30% of all tornado outbreaks. The
22 impacts of WR persistence on tornado activity anomalies, however, are found to be asymmetric:
23 compared to non-persistent WRs, persistent WRs amplify positive tornado activity anomalies but
24 may not further enhance negative tornado activity anomalies. An empirical model using WR
25 frequency and persistence captures the year-to-year variability of warm-season tornado days and
26 outbreaks reasonably well, including some years with high-impact outbreaks. Our study
27 highlights the potential application of WRs for better seasonal prediction of tornado activity.

28 **1.1 Introduction**

29 The contiguous United States (CONUS) experiences more tornadoes than anywhere else in the
30 world, leading to significant economic and life losses (NCEI, 2024). Tornado outbreaks (TOs)
31 are a primary contributor to these impacts, and the annual frequency has increased by 2.5 events
32 over the past 63 years (Brooks et al. 2014; Graber et al. 2024), particularly over the Southeast
33 U.S. (Gensini and Brooks, 2018; Graber et al., 2024; Moore, 2018; Moore and DeBoer, 2019). In
34 contrast, tornado days (TDs) have decreased in frequency at a rate of ~ 10 per decade since 1960
35 (Brooks et al. 2014; Graber et al. 2024), especially from March to September, and over the
36 southern Great Plains (Gensini and Brooks, 2018; Graber et al., 2024; Moore, 2018; Moore and
37 DeBoer, 2019). Embedded within these trends is large interannual variability, as evidenced by
38 the percent change, with respect to the previous year, in annual CONUS tornado reports over the
39 recent five years (2019-2023): +34.7%, -28.7%, +21.4%, -13.0%, and +24.5%, as well as by the

Style Definition: Default Paragraph Font

Formatted: Font: Italic

Formatted: Numbered + Level: 1 + Numbering Style: 1, 2, 3, ... + Start at: 1 + Alignment: Left + Aligned at: 0" + Indent at: 0.25"

corresponding percent change in tornado fatalities: +320.0%, +80.9%, +36.8%, -77.9%, and +260.9% (Storm Prediction Center, 2024). Such variability affects the situational awareness and vulnerability of the populations, especially those that are disadvantaged. It also complicates decision making and resource management by key stakeholders across multiple sectors. In addition, exposure to future tornadoes is increasing with growing urban areas (Ashley and Strader, 2016; Strader et al., 2017, 2024). These and other impacts motivate the efforts to better understand the variability of tornado activity over the seasonal and longer time scale, which would ultimately contribute to improved prediction of tornado activity.

Some variability of tornado activity can be attributed to low-frequency climate modes (Miller et al., 2022; Niloufar et al., 2021; Thompson and Roundy, 1998; Vigaud et al., 2018). ~~For example, Lee et al. (2016) found that La Niña (El Niño) years typically coincide with increases (decreases) in tornado activity in tornado-prone regions over the United States due to ENSO effects on the jet streams (Cook et al., 2017). For example, Cook and Schaefer, (2008) examined winter tornado outbreaks in relation to the phase of the El Niño – Southern Oscillation (ENSO) and found that a La Niña phase favored tornadoes in the Southeast and a neutral phase favored tornadoes in the Great Plains. Allen et al., (2015) further found that La Niña (El Niño) years typically coincide with more (fewer) tornadoes in the spring across the central CONUS, and that the winter ENSO phase can be used to predict tornado frequency during the spring.~~ Additionally, a positive (negative) phase of the Arctic Oscillation (AO) combined with a La Niña (El Niño) phase may increase (decrease) ~~in~~ tornado activity (Tippett et al., 2022). Tornado activity can also be modulated by anthropogenic climate change (ACC), either indirectly via changes in climate modes, ~~such as through an increase in consecutive La Niña years in a warming climate (Geng et al., 2023), or/and directly via changes in relevant atmospheric conditions. or/and directly via changes in relevant atmospheric conditions.~~ For example, increasing greenhouse gas concentrations are projected to lead to a moister atmosphere, especially in the lower troposphere, which in turn contributes to higher convective available potential energy (CAPE) (Trapp et al., 2007). Diffenbaugh et al. (2013) showed that climate models project a robust increase in the number of days with high CAPE coinciding with high vertical wind shear (VWS) in the eastern U.S., two important parameters for tornado-favorable environments (Brooks et al., 2003; Mercer and Bates, 2019; Rasmussen and Blanchard, 1998; Thompson et al., 2012).

Variability of synoptic-scale circulations provides another means of explaining tornado activity. Conductive synoptic-scale circulation anomalies for TOs in the United States show a trough-ridge pattern over the central- to eastern-CONUS, while non-TOs usually feature more zonal flow and weaker relative vorticity (Mercer et al., 2012). In particular, Cwik et al. (2022) performed rotated EOF analysis of 500-hPa geopotential height associated with historic May TOs and identified three circulation patterns. The three circulation patterns are all characterized by a trough feature over the central to eastern U.S. While their study concludes that the synoptic patterns associated with TOs remain the same over time, there is partial variability in the locations of TOs on multidecadal scales. Additionally, mesoscale processes without strong links to synoptic-scale

circulations also affect tornadoes, especially weak or isolated tornado events (e.g., tornadogenesis in non-supercellular storm modes associated with mesoscale boundaries; see Wakimoto and Wilson, 1989).

In this study, we will investigate the link between the synoptic-scale circulation and tornado activity using the concept of weather regimes (WRs). ~~Different from EOF analysis, WRs), identified using the K-means clustering analysis are not required to be orthogonal to each other, which can more flexibly represent various recurrent synoptic scale circulation patterns.~~ Previous studies suggest that WRs represent a finite number of equilibrium states of the climate system (Charney and DeVore, 1979; Hannachi et al., 2017; Michelangeli et al., 1995). Their spatial patterns are determined by the internal dynamics of the atmosphere, while their frequencies and persistence may be modulated by climate modes or external forcings such as ACC (Corti et al., 1999). ~~The WR framework thus has a strong dynamic basis.~~ The WR framework thus has a strong dynamic basis and have been used to reliably detect changes in regional temperature and precipitation (Robertson and Ghil, 1999). Additionally, unlike Cwik et al. (2022)'s study, which focuses on circulation patterns conditioned on major TOs, our identification of WRs is independent of TOs. This approach allows us to examine WRs that facilitate or hinder tornado activity, providing more comprehensive information for potential forecasting applications. Furthermore, we will examine environmental conditions relevant to tornado development, such as CAPE and VWS (Brooks et al., 2003; Mercer and Bates, 2019; Rasmussen and Blanchard, 1998; Thompson et al., 2012), which will help us better understand the link between WRs and tornado activity.

WRs were used previously to investigate sub-seasonal variability of tornado activity, and a skillful WR-based, hybrid model was developed for the sub-seasonal prediction of tornado activity in the month of May (Miller et al. 2020). ~~Year-round WRs (Lee and Messori, 2024) have also been used and found to have statistically significant relationships with tornado activity in all months except June-August (Tippett et al. 2024) although without any~~ Lee et al., (2023) applied the year-round WR method (Grams et al., 2017) over North America and defined four year-round WRs. Tippett et al., (2024) identified statistically significant relationships between these year-round WRs and tornado activity in all months except June through August, but Tippett et al. (2024) made no consideration of WR persistency. This helps motivate our focus herein on the warm-season tornado activity and its interannual variability. We will test the hypothesis that the interannual variability of warm-season tornado activity is modulated by WR frequency and persistence. A better understanding of the possible links between WRs and tornado activity may contribute to improved seasonal prediction of tornado activity.

2.2 Data and Methodology

2.1 ERA-5 reanalysis data

~~500 hPa geopotential heights (500H) and parameters, including most unstable CAPE (MUCAPE), 10m and 500 hPa winds, and convective precipitation (CP), from~~ Using the ERA-5

Formatted: Numbered + Level: 1 + Numbering Style: 1, 2, 3, ... + Start at: 1 + Alignment: Left + Aligned at: 0" + Indent at: 0.25"

reanalysis dataset (Hersbach et al., 2020), 500 hPa geopotential heights (500H) and parameters including most unstable CAPE (MUCAPE), 10m and 500 hPa winds, and convective precipitation (CP) were analyzed over the CONUS [24 – 55° N, 130 – 60° W] using the native 0.25° × 0.25° (latitude × longitude) resolution. Since the tornadic storms leading to TOs tend to initiate between 18 and 00 UTC after sufficient atmospheric destabilization from surface heating (Cwik et al., 2022), 500H at 21 UTC was used to represent the daily circulation patterns. Daily maximum values of MUCAPE and CP at each grid point were used to represent the daily peak instability and to avoid too many near-zero CP values in a daily mean in turn amplify the signal for days with the potential for significant convective storms. The 0-6 km bulk wind shear (S06), or deep-layer shear, was estimated at each grid point and 3-h interval as the magnitude of the vector difference between the 500 hPa and 10 m winds. The daily mean S06 was then determined at each ERA-5 grid point. Daily anomalies of MUCAPE, S06, and CP were calculated by subtracting each calendar day's mean from every calendar day, following

$$H'(d, y) = H(d, y) - \bar{H}(d) \quad (1)$$

where y is year, d is calendar day, H is the variable or parameter of consideration, and the overbar denotes the long-term mean.

Following Graber et al. (2024), all analyses were conducted over the period 1960-2022, and focused specifically on the warm season, defined as April to July, which is peak season of tornado activity.

2.2 Weather Regimes

To identify weather regimes, the seasonal cycle, defined as the long-term mean of 21 UTC 500H at each grid-point for each calendar day, was removed. The 500H data were then detrended by removing the linear trend of the warm-season seasonal mean (AMJJ) 500H averaged over the entire Northern Hemisphere (Fig. S1). The detrending approach removed the positive trend of hemispheric mean 500H caused by climate change while preserving the spatial patterns and potential changes of WR frequency or persistence. K-means clustering analysis was then applied. While many previous studies applied a low-pass filter or/and EOF dimension reduction prior to K-means clustering analysis (e.g., Grams et al., 2020; Lee et al., 2023; Lee and Messori, 2024; Robertson et al., 2020), Falkena et al., (2020) cautioned against the use of either EOFs or time filtering on top of K-means clustering. Our analysis shows that the application of the 5-day running mean or EOF dimension reduction prior to K-means does not qualitatively affect the regime patterns or the regime frequencies (Figs. S2-S4). We thus chose to use the simplest procedures for regime classification. Additionally, unlike Tippett et al., (2024), 500H anomalies are not normalized as we focus on one season, so seasonality is not as much of a concern. K-

means clustering analysis was applied to the 500H daily anomalies over the CONUS, and the number of clusters was determined as five using the elbow method (Miller et al. 2020; Kodinariya and Makwana 2013). A persistent WR was defined as a WR lasting for ≥ 5 consecutive days. ~~It is worth mentioning that different from the EOF analysis by Cwik et al. (2022), WRs identified using K-means clustering analysis are not required to be orthogonal to each other. WRs can thus more flexibly represent various recurrent synoptic-scale circulation patterns.~~

2.3 Tornado Reports

Tornado reports ~~for the period 1960-2022~~ were obtained from the NOAA Storm Prediction Center Severe Weather Database. These reports are georeferenced with time, date, and EF/F rating. TDs were defined as any day with ≥ 1 EF/F-1+ tornadoes, and TOs were defined as any day with >10 EF/F-1+ tornadoes. The >10 threshold provides a larger sample size than higher thresholds but has a similar trend as >20 or >30 thresholds (Graber et al. 2024). ~~Early reporting in the 1960s has known biases, and EF/F-0 reports were not included due to their reporting uncertainty (Brooks et al., 2014; Trapp, 2013). Despite the increase in weak tornado reports in the 1990s due to the deployment of the NEXRAD radar system (Bieringer and Ray, 1996), this trend is not reflected in TDs. Nevertheless, there are remaining and well-known biases in this dataset, which we attempt to manage with a focus on days with tornadoes rather than tornado counts (e.g., Brooks et al. 2014; Graber et al. 2024; Trapp, 2014).~~

The TD probability anomalies (P_a) were calculated at each grid-point for each WR as follows:

$$P_a = \frac{P_i - P_c}{P_c} \times 100 \quad P_a = \frac{P_t - P_o}{P_o} \times 100 \quad (+2)$$

where P_c is the climatological mean TD probability and was calculated as the total number of TDs divided by the total number of days in the warm-season from 1960-2022, and P_i represents the TD probability for WR- i (i.e., the number of TDs for WR- i divided by the total WR- i days). WRs that are (are not as) conducive for TDs would have probabilities above (below) the climatological mean and thus positive (negative) probability anomalies. The probability anomalies of TOs and the probability anomalies associated with persistent and non-persistent WRs were calculated similarly. ~~A Monte Carlo simulation test with 10000 resamples was used to test for significance of the anomalies. The number of WR- i days was multiplied by the climatological mean TD probability to get an expected number of tornado days. The p-value was calculated based on the proportion of simulations that were more extreme than the observations.~~

2.4 Empirical model for tornado activity

Using WR frequency and tornado probabilities for both persistent (subscript p) and non-persistent (subscript np) WRs, we developed an empirical model to assess the relationship between the variability of seasonal tornado activity and WRs:

Formatted: Font: 12 pt, Italic

Formatted: Font: 12 pt

Formatted: Font: 12 pt, Italic

Formatted: Font: 12 pt

Formatted: Font: 12 pt, Italic

Formatted: Font: 12 pt

Formatted: Font: 12 pt, Italic

Formatted: Font: 12 pt

Formatted Table

$$TI(t) = \sum_{i=1}^5 f(i, t)_p \times P_{i,p} + \sum_{i=1}^5 f(i, t)_{np} \times P_{i,np}$$

$$TH(t) = \sum_{i=1}^5 f(i, t)_p \times P_{i,p} + \sum_{i=1}^5 f(i, t)_{np} \times P_{i,np}$$

(2)
(3)

Formatted Table

where $TI(t)$ denotes a tornado index for year t . The model takes the count of WR- i days ($f(i, t)$) for year t and multiplies it by the tornado probability corresponding to WR- i ($P(i)$). The WR count is a function of regime (i) and year (t). The WR tornado probability is only a function of regime (i) and represents the likelihood that a TD will occur. Probabilities are assessed for persistent and non-persistent WRs separately, under the hypothesis that persistent WRs contribute to stronger TD or TO anomalies (Miller et al., 2020; Trapp, 2014). Spearman Rank correlation is used to compare the modeled and observed tornado indices.

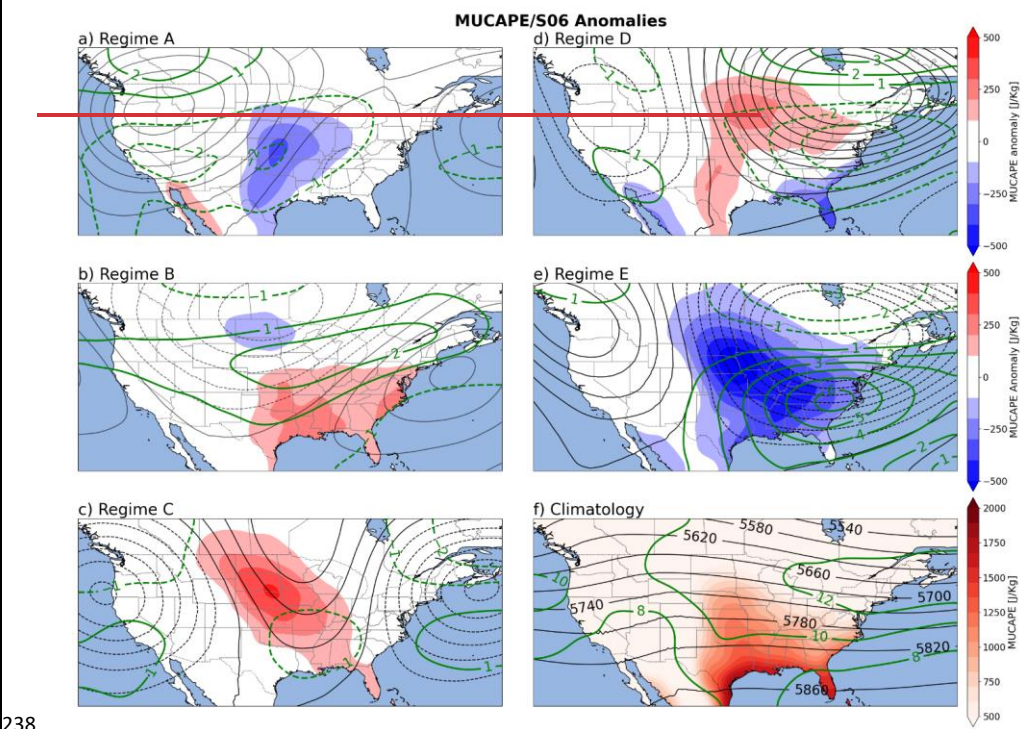
3. Weather Regimes and Tornado Activity

The composite mean 500H anomalies for each WR are shown in Fig. 1, ordered with decreasing frequency of occurrence. WR-A is the most frequent regime and is characterized by an anomalous high over the west-central-CONUS and a weak anomalous low over the Southeast. WR-B and WR-C are both characterized by a three-cell wave pattern, with negative and positive 500H anomalies over the central-CONUS, respectively. WR-D and WR-E are west-east dipole patterns that nearly mirror each other. ~~These WRs have some spatial similarities to the year-round WRs found by Lee and Messori, (2024), with WR-A reflecting a Pacific Trough, WR-B and WR-D showing warm and cool phases of a Pacific Ridge associated with ENSO, and WR-E reflecting an Alaskan Ridge. Some WRs are similar to the year-round WRs in Lee et al., (2023), which were subsequently used by Tippett et al., (2024). More specifically, WR-A features spatial similarities to a Pacific Trough, WR-B and WR-D show warm and cool phases of a Pacific Ridge associated with ENSO, and WR-E is characterized by an Alaskan Ridge. WR-C features spatial similarities to a Greenland High as well. It is worth mentioning that our study focuses on a different region, a specific season and chooses a different k value, and there are thus noticeable differences. WR-A features two anomalous highs over the two coasts as opposed to one anomalous high over the central-CONUS. The anomalous low in WR-B is more pronounced than in Lee et al., (2023). The anomalous high in WR-C is wavelike unlike the Greenland high in Lee et al., (2023). The dipoles in WR-E are further south than they are in the Alaskan Ridge in Lee et al., (2023).~~

The potential links between these WRs and tornado activity are indicated by MUCAPE and S06 (Fig. 1a-e). Composite anomalies of these parameters were calculated by subtracting the corresponding climatological mean (Fig. 1f) from the composite mean associated with each WR. The high values of the climatological MUCAPE across the central- and southeastern CONUS are connected to the physical geography of North America (Brooks et al., 2003; Trapp, 2013) and the warm-season climatological mean 850-hPa circulation, with southerly winds transporting heat and moisture into the central-CONUS (Mercer and Bates, 2019). The climatological S06 is

Formatted Table

221 characterized by high values over the eastern-CONUS, which are tied to the midlatitude jet
 222 stream. With an anomalous high over the west-central-CONUS and an anomalous low over the
 223 Southeast, WR-A favors anomalously low MUCAPE and S06 relative to climatological means.
 224 In contrast, the anomalous low over central North America and the anomalous high over the
 225 southeastern U.S. in WR-B imply enhanced westerly flow and increased moisture and warm-air
 226 transport from the Gulf, leading to positive S06 and MUCAPE anomalies in southeastern U.S.
 227 The favorable anomalies presented in WR-B agree with the Pacific Ridge findings in Tippett et
 228 al. (2024). In WR-C, the anomalous low over western North America and the anomalous high
 229 over central North America imply enhanced southerly flow and increased moisture and heat
 230 transport leading to positive MUCAPE anomalies in the central U.S., which overlap with
 231 reduced S06 south of the anomalous high. For WR-D, the anomalous high over the eastern
 232 CONUS and the anomalous low over the western CONUS imply enhanced southerly flow and
 233 increased moisture and heat transport, consistent with positive MUCAPE anomalies in the
 234 central U.S., while S06 decreases in the south of the anomalous high and increases in the north.
 235 WR-E, in contrast to WR-D, implies reduced southerly flow and decreased moisture and warm-
 236 air transport and is associated with negative MUCAPE anomalies in the central U.S., but S06
 237 increases substantially over the Southeast.



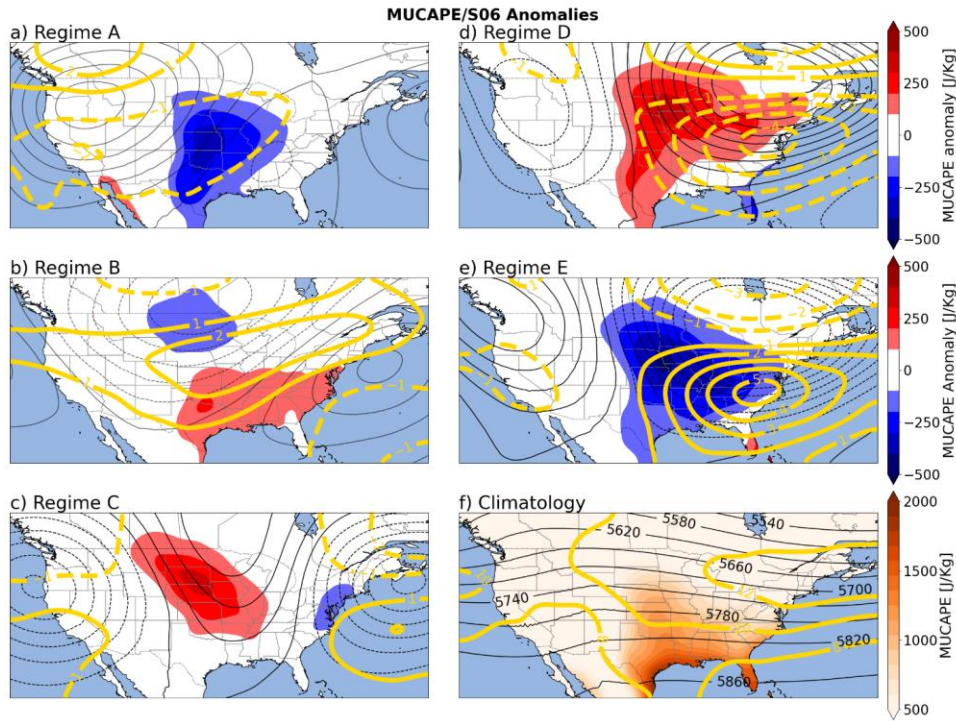
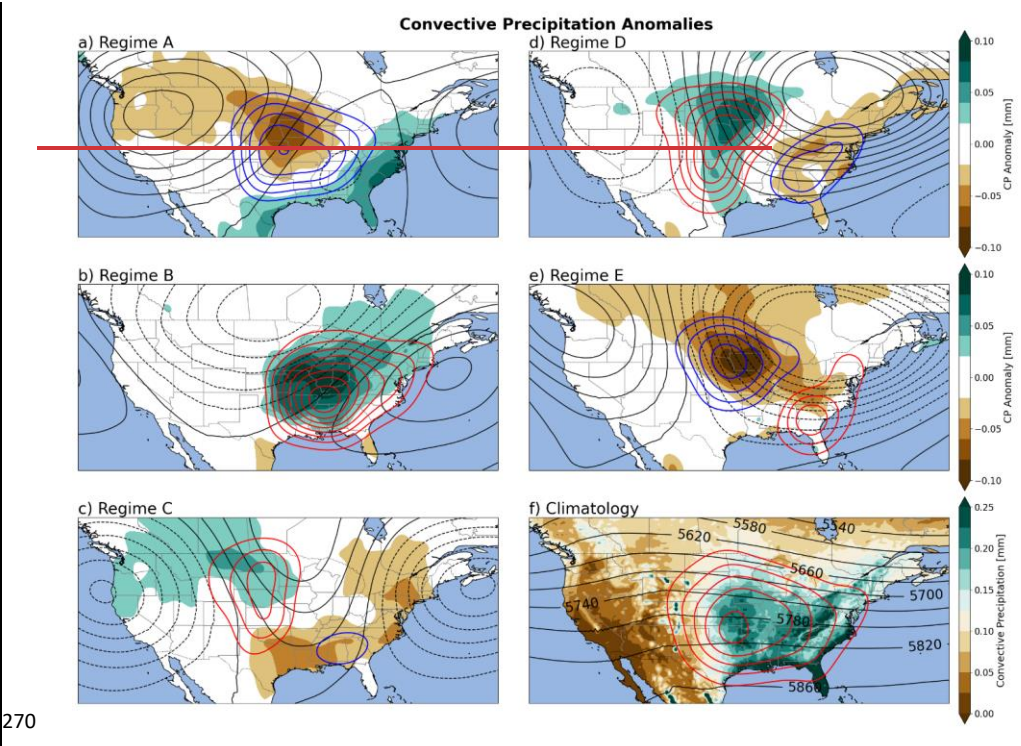


Figure 1: (a-e) Composite anomalies of 500H (black contours, ± 10 m) for each warm-season WR and corresponding anomalies of daily maximum MUCAPE (units: J Kg^{-1} ; color fill) and daily mean S06 (units: m s^{-1} ; green/gold contours); (f) Warm-season climatology of 500H (black contours), daily maximum MUCAPE (color fill) and daily mean S06 (green/gold contours).

The WR-tornado activity link is illustrated by the composite anomalies of TD probability and CP for each WR. The climatological TD probability and CP are also shown (Fig. 2f) for reference. Here TD probability anomalies are evaluated following Eq. 42 with respect to P_c at each grid point. Convective-storm occurrences can be approximated using CP. Convective storms are a necessary but insufficient condition for tornadoes, so more CP does not necessarily lead to more tornadoes, but less CP likely means reduced tornado activity (Tippett et al., 2014). CP anomalies collocate well with the MUCAPE anomalies (Fig. 1) since non-zero CAPE is generally necessary for deep convection, but CP also includes information about convection initiation. WR-A has negative TD anomalies in the central-CONUS, where negative anomalies in CP and MUCAPE/S06 are also present. Positive TD anomalies in the Southeast and Midwest of WR-B are collocated with positive anomalies in CP, MUCAPE, and S06. Despite the negative S06 anomalies, positive TD anomalies occur in the central Great Plains in a region of positive MUCAPE and CP anomalies for WR-C. Weak, negative TD anomalies in association with WR-

258 C are found in the Southeast where negative CP anomalies are present. Positive (negative) TD
 259 anomalies in WR-D over the central-CONUS are collocated with positive (negative) CP and
 260 MUCAPE anomalies, and reduced S06 (Fig. 1d) also contributes to the negative TD anomalies in
 261 the Southeast. Finally, negative TD anomalies occur in the central-CONUS, collocated with
 262 negative anomalies of MUCAPE and CP associated with WR-E, while positive TD anomalies
 263 occur in the Southeast despite reduced MUCAPE. The latter can probably be attributed to the
 264 strong positive anomalies in S06 ~~and may be possibly linked to tropical cyclones (Figs. (Figs. 1e~~
 265 ~~and 2e).~~ However, given the low climatological TD probability in the Southeast (Fig. 2f), the
 266 absolute changes in TD days may not be high. Overall, the distribution of TD anomalies shows a
 267 good agreement with CP and MUCAPE anomalies of the same sign, and S06 seems to play a
 268 secondary role in most regions.

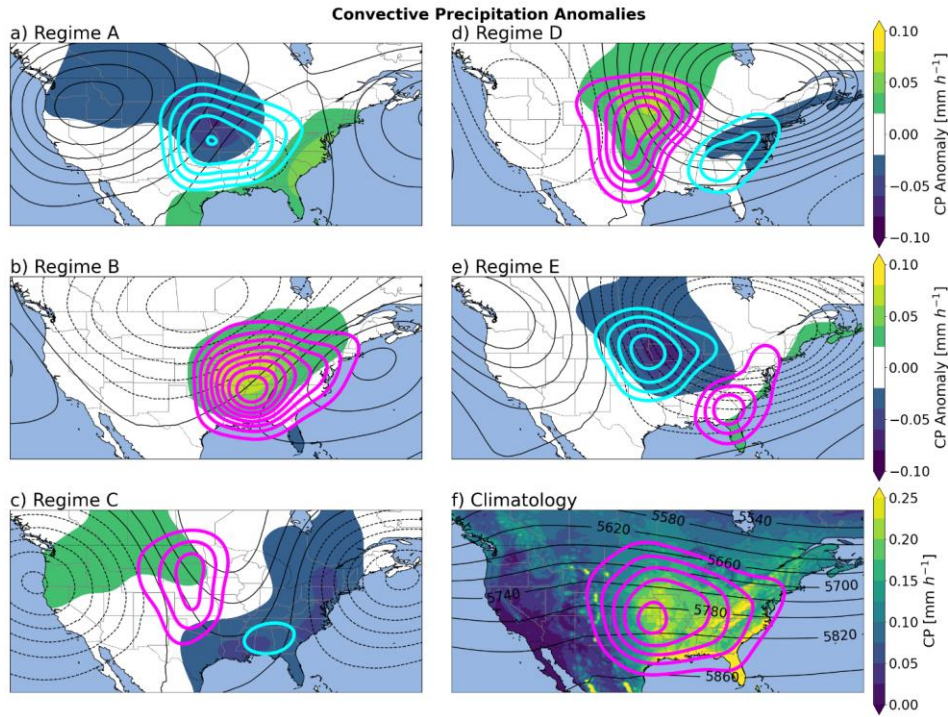
269



270

271

Fig.



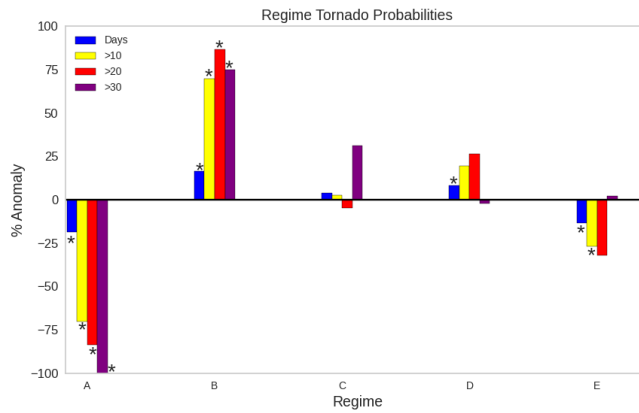
272

273 **Figure 2:** a-e): Significant composite anomalies of daily maximum CP rate (units: mm h⁻¹; shading) at each grid
 274 point (green/brown/blue filled contours) for each WR A-E days with TD probability anomalies (contour intervals: +/-
 275 10 %; red/magenta and blue/cyan colors represent positive and negative values, respectively) and 500hPa for each WR
 276 (black contours: +/- 10 m); (f) Climatology of daily maximum CP (shading), 500hPa (black contours), and tornado
 277 day probability (red/magenta contours). Significance is tested at each grid point using Student's one-sample t-test
 278 with the null hypothesis that the sample mean of the anomalies is equal to zero, and anomalies with p-values ≤ 0.05
 279 are regarded as significant.

280 The link between WRs and geospatially aggregated tornado activity is summarized in Fig. 3 for
 281 different regions. There are a total of 4348 warm-season TDs from 1960-2022, therefore $P_c \approx$
 282 56.5%. TD probability is enhanced for WR-B and WR-D, with probability anomalies of **16.5%**
 283 and **8.2%**, respectively (corresponding to TD probabilities of **65.9%** and **61.3%**; Fig. 3). For
 284 reference, these are associated with large positive TD probability anomalies in the Southeast and
 285 central-CONUS, respectively (Fig. 2). TD probability is reduced for WR-A and WR-E,
 286 associated with negative tornado-report anomalies across the central-CONUS (Fig. 2). The TD
 287 probability anomaly associated with WR-C is close to zero (Fig. 3), which can be attributed to
 288 the cancellation between the opposite anomalies in the Southeast and central-CONUS (Fig. 2).

289 There are 415 warm-season TOs from 1960-2022, therefore $P_c = 5.4\%$. In general, the TO
 290 probabilities have a stronger signal than TDs (yellow bars in Fig. 3). For TOs, WR-A has the
 291 strongest negative signal with a **-70.01%** anomaly while WR-B has the strongest positive signal
 292 with a **+69.81%** anomaly (Fig. 3). The TO anomalies are consistent with the analysis in Figs. 1-
 293 2, in which WR-A (WR-B) showed reduced (enhanced) MUCAPE, S06, and CP over the central
 294 and Southeast CONUS. The TO probability associated with WR C is around the climatological
 295 mean. WR-D has a positive, but not significant anomaly of TO probability (**+19.56%**; Fig. 3),
 296 which is consistent with enhanced MUCAPE and CP over the central-CONUS (Figs. 1d&2d).
 297 WR-E is associated with a negative TO probability anomaly, which can be linked to the reduced
 298 tornado activity over the central-CONUS (Fig. 2). Further analysis reveals that roughly **83%** of
 299 all TOs occur during a WR-B, C, or D.

300 We also checked TOs using >20 and >30 tornadoes thresholds (red and purple bars in Fig. 3).
 301 The analysis based on the >20 threshold yields similar results as that defined based on the >10
 302 threshold. Although WR-A and WR-B demonstrate significant and consistent signals for days
 303 with >30 tornadoes, the other WRs exhibit contrasting signals for the >10 and >30 thresholds.
 304 This could be due to the small sample size of TOs when using the >30 threshold, and those
 305 anomalies are not significant.



306
 307 **Fig. Figure 3:** Tornado probability anomalies for days with > 0, > 10, > 20, & > 30 tornadoes for each WR in the
 308 CONUS (see Eq. 42 and the related discussion). Anomalies above the 95 % confidence level based on the Monte
 309 Carlo testing (with 10,000 resampling) are regarded as significantly different from zero and marked with an asterisk.

310 Next we compare persistent and non-persistent WRs to test the hypothesis that persistent regimes
 311 amplify the TD/TO probability anomalies. Persistent WRs are defined as those lasting for at least
 312 5 days. The comparison of the TD probability anomalies between persistent and non-persistent
 313 WRs (Fig. 4a) does not fully support our hypothesis. Although persistent WR-B and WR-D are
 314 associated with a stronger positive anomaly in TD probability than their non-persistent
 315 counterparts, the negative TD probability anomalies are about the same for persistent and non-
 316 persistent WR-A, and persistent WR-E shows an even weaker decrease in TD probability than

non-persistent WR-E. Persistent and non-persistent WR-C show TD probability anomalies of opposite signs, both with a small magnitude. Compared to TD probability, the anomalies of TO probability are generally stronger for both persistent WRs and non-persistent WRs. In particular, persistent WR-B is associated with an increase of TO probability by close 80% and accounts for about 30% of all TOs, while persistent WR-A is associated with a decrease of TO probability by about 70%. However, a consistent picture emerges: persistent WRs amplify the positive anomalies but do not further enhance the negative anomalies in comparison to the corresponding non-persistent WRs. The exception is persistent WR-C, which is associated with nearly zero TO anomaly, in contrast to a positive but not significant anomaly for non-persistent WR-C (Fig. 4b).

The asymmetric impacts of WR persistence on positive and negative tornado activity anomalies are also illustrated in Fig. S2S5. One possible interpretation is that tornado activity indices are positively defined metrics so they cannot be reduced much further when already close to zero. Additionally, the results should also be interpreted with caution given the limited sample sizes for certain groups (Table S1).

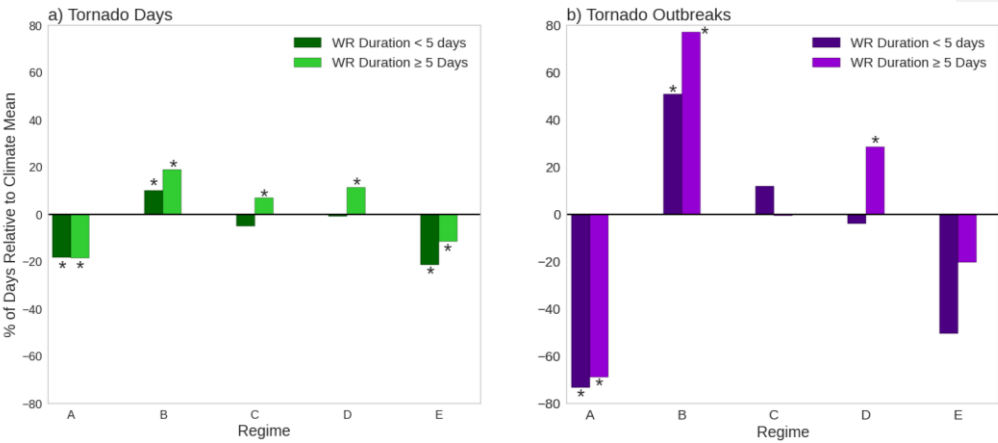


Fig. Figure 4: (a) TD and (b) TO (days with > 10 EF-1+ tornadoes) probability anomalies for each WR for persistent and non-persistent days. Anomalies above the 95 % confidence based on the Monte Carlo testing are marked with an asterisk. Anomalies above the 95 % confidence level based on the Monte Carlo testing (with 10,000 resampling) are regarded as significant and marked with an asterisk.

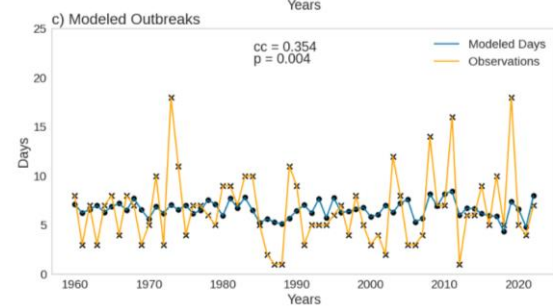
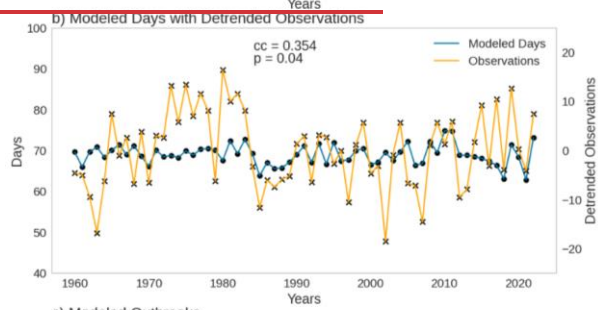
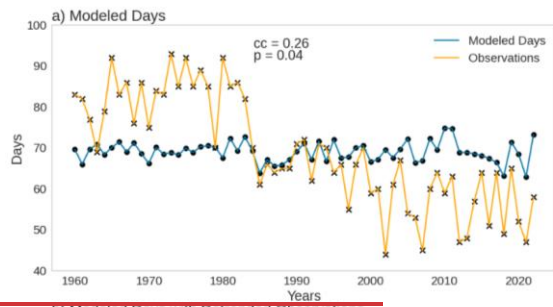
4. Variability of WRs and Tornado Activity

In this section, we further quantify the link between WRs and tornado activity. WR frequencies demonstrate strong interannual and decadal variability (Fig. S4aS6a-e). In particular, WR-A exhibits a frequency increase during the 1980s and reached a peak around 1990, coinciding with the steepest decrease in TDs (Brooks et al., 2014; Graber et al., 2024); and WR-D shows a

negative trend of occurrence in the recent two decades. The frequencies of persistent WRs also show changes across different multidecadal time periods (Fig. S4fS6f).

To examine whether WRs can help explain the interannual and decadal variability of tornado activity over the period 1960-2022, an empirical model was developed following Eq. 2-3. Figure 5a shows the empirically modelled TDs along with the observed TDs. Despite the decadal variability of WR and persistent WR frequencies (Fig. S4S6), the empirical model fails to capture the observed decreasing trend or the decadal shift in the 1980s. After detrending the observations using the least-squares fit, the model reasonably represents the interannual variability of TDs (Fig. 5b), with a rank correlation of **0.35** (p-value ~0.04). An empirical framework for EF-3+ TDs was also tested, yielding a rank correlation of **0.37** (Fig. S5S7). It is interesting to note that the modelled TDs are nearly out of phase with observations in the 1960s, when tornado reports are less reliable (Trapp, 2013). After excluding these years, we reconstructed the empirical model using updated TD probabilities during 1970-2022, and the correlation increases to **0.46** (Fig. S6aS8a). The empirical framework was also tested for EF-3+ TDs during 1970-2022, and the correlation is **0.49** (Fig. S6bS8b).

We also examined TOs. The ~~TO time series from the empirical model picks up the interannual variability of the observed TOs with has a significant rank correlation of 0.36, although (above the 95% confidence level) with the magnitude of the variability is underestimated (Fig. 6e), which is a typical limitation of statistical models observations but it underestimates the observed variance.~~ Since the observed TOs do not have a strong trend, detrending the data does not affect the results appreciably. Similar to the TD model results (Fig. 5a, b), the TO model is nearly out of phase with the observations in 1960s. After excluding the data in 1960s, the correlation between the empirical model and observation increases to **0.43** from 1970-2022 (Fig. S6eS8c).



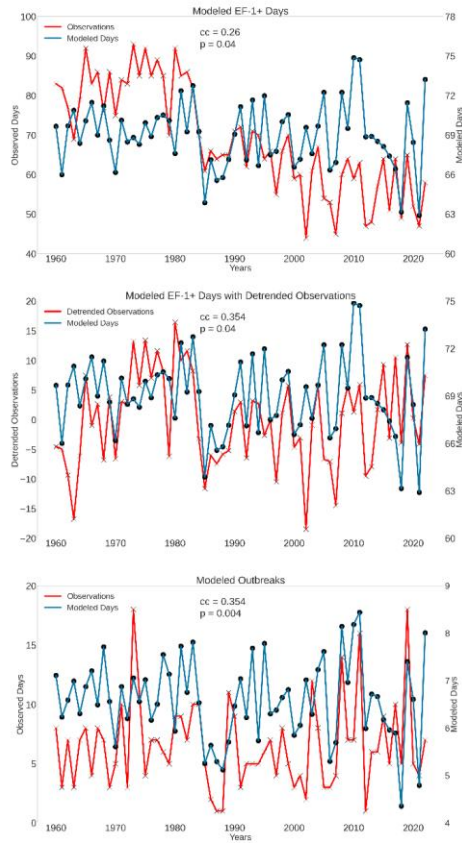
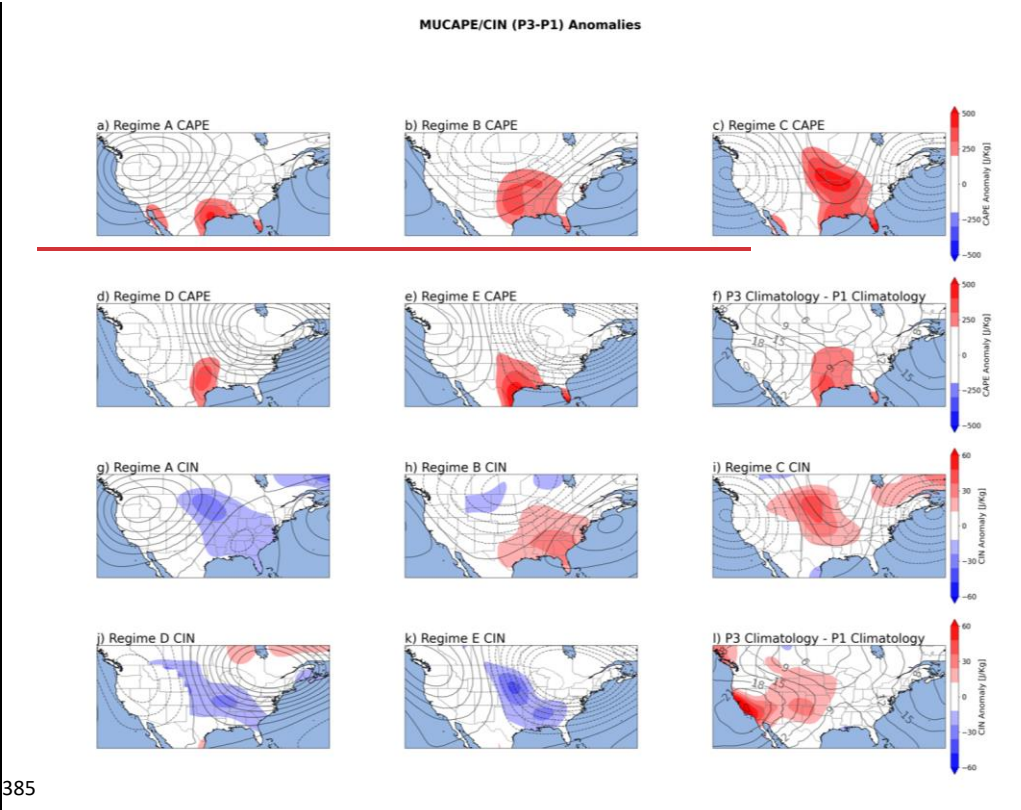


Fig.

Figure 5: Empirically modeled TDs (blue with circles) per year overlaid with (a) observed TDs (yellowred with crosses) and (b) detrended observed TDs (yellowred with crosses) with spearman rank correlation coefficient (cc) and p-value; (c) empirically modeled (blue with circles) and observed (yellowred with crosses) TOs per year with the spearman rank correlation coefficient and p-value.

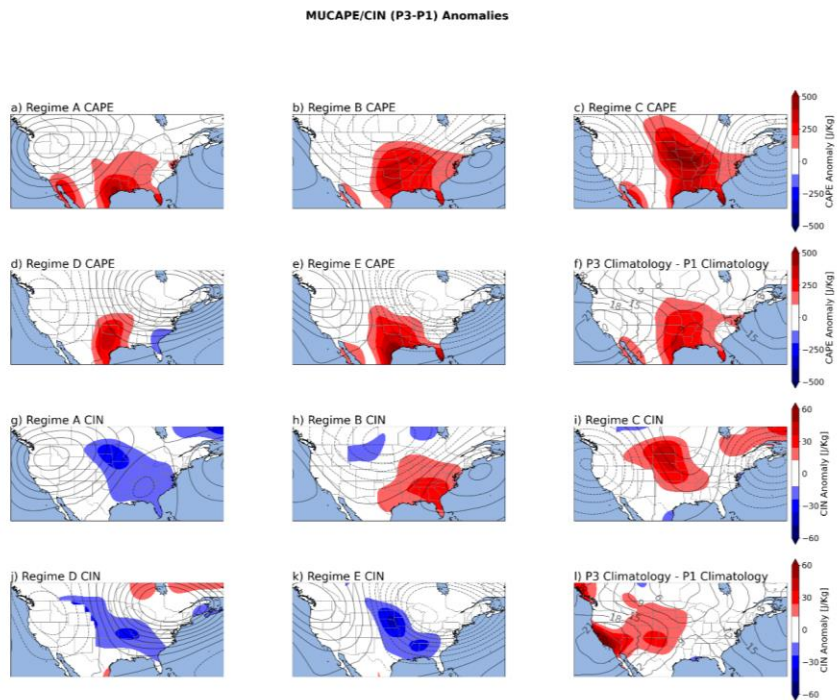
It is worth noting that although the empirical model captures the interannual variability of TDs reasonably well, it misses the negative trend or decadal variability of TDs. The empirical model is constructed under the assumption that probability anomalies of tornado activity associated with the WRs do not change during the period of analysis. This assumption, however, may not be strictly valid. For example, MUCAPE increases over time for all five WRs, although S06 undergoes smaller changes (Fig. 6a-f, S7-S8S9-S10). Additionally, convective inhibition (CIN) increases in the Southeast for WR-B (Fig. 6h) and in the central-CONUS for WR-C (Fig. 6i) from P1 to P3. Further analysis reveals lower TD probability for various regimes in P3 than in P1 (not shown). This may explain why the empirical model fails to capture the trend of TDs. A better understanding of dynamic and thermodynamic anomalies associated with WRs and the

383 role of internal climate variability and anthropogenic forcing in modulating WRs will help us
384 better understand tornado activity on the decadal and longer time scales.



385

386 **Fig.**



387
388 **Figure 6:** Change in MUCAPE (shading) anomalies (a-e) and CIN (shading) anomalies (g-k) from period 1 (1960-
389 1979) to period 3 (2000-2022) for each WR and (f, l) all WR days.

390 **5. Summary**

391 The weather regime concept was used to investigate the link between synoptic-scale circulation
392 patterns during the warm season and the variability of corresponding tornado activity over the
393 U.S. on the interannual time scale. Five WRs were identified over North America using the K-
394 means clustering analysis of daily 500H anomalies from the ERA-5 reanalysis. WR-A is a three-
395 cell wave-pattern and is associated with negative anomalies of tornado activity in the central-
396 CONUS, which is consistent with negative anomalies of MUCAPE and S06 over that region.
397 WR-B is a three-cell wave-pattern that contributes to increased tornado activity in the Southeast
398 as evidenced by positive anomalies in MUCAPE and S06 there. WR-C is a three-cell wave-
399 pattern with negative 500H anomalies over both coasts. It is associated with positive MUCAPE
400 anomalies over the central-CONUS and negative S06 anomalies. It exhibits climatologically
401 average tornado activity, but it does make a positive, spatially small, contribution to tornado

402 activity in the Great Plains. WR-D and WR-E are both dipole patterns with positive and negative
403 500h anomalies over the east coast, respectively. WR-D contributes to anomalously positive
404 tornado activity in the Great Plains while WR-E contributes to anomalously negative tornado
405 activity in the Great Plains. WR-E also contributes to positive anomalies of tornado activity in
406 the Southeast, ~~possibly linked to tropical cyclones.~~ A year that includes a high number of WR-
407 B days is likely to have an above average number of TDs and TOs. In contrast, a year with a high
408 number of WR-A days would likely have a below average number of TDs and TOs

409 We tested the hypothesis that WR persistence amplifies the tornado activity anomalies,
410 regardless of positive or negative anomalies. However, the impacts of WR persistence on
411 positive and negative tornado activity anomalies are found to be asymmetric: persistent WRs
412 amplify the positive anomalies but may not further enhance the negative anomalies. This can
413 probably be attributed to the positive-definite nature of tornado activity indices. While persistent
414 WRs with favorable environmental conditions (such as WRs B and D) may further increase
415 tornado activity, TD or TO probability cannot be reduced much further by the persistence of a
416 tornado-unfavorable WR (such as WR-A) when they are already close to zero.

417 Using WR frequency and persistence, an empirical model was developed to quantify the
418 relationship between tornado activity and warm-season WRs. The performance of the empirical
419 model shows promising skill in estimating the interannual variability of tornado days or TO
420 days, and the model performance was better after excluding the data in the 1960s. The empirical
421 model, however, misses the trend or the multi-decadal variability of TDs. This model deficiency
422 could be attributed to the non-stationary relationship between WRs and tornado activity on the
423 multi-decadal time scale, which is illustrated by the increase in CAPE for all WRs in the more
424 recent decades. The roles of internal variability and anthropogenic forcing, however, ~~is~~are
425 outside the scope of the present study and merit further investigation. Furthermore, although not
426 explored in this study, WRs and tornado activity may both be modulated by large-scale, low-
427 frequency climate modes. WRs could potentially act as an intermediary between large-scale
428 climate modes and tornado activity, while the low-frequency modes may be important sources of
429 predictability for the interannual variability of tornado activity. Overall, weather regimes offer a
430 promising path for developing skillful seasonal tornado prediction models. Such efforts are
431 ongoing and will be reported in due course.

432

433

434

435

436

437

438

439

Formatted: Font: Bold

440

441 **Code Availability**

442 Weather Regime identification code is available at:

443 <https://github.com/Matt0604/Kmeans>

444

445

446 **Data Availability**

447 The ERA5 data are available at the NCAR research data archive (RDA) (ds 633.0) and

448 Copernicus Climate Data Store (CDS).

449 doi: 10.5065/BH6N-5N20

450 The tornado report data used in this study are available through the NOAA Storm Prediction

451 Center severe weather database.

452 <https://www.spc.noaa.gov/wcm/#data>

453

454 **Author Contributions**

455 Conceptualization: ZW, RJT, MG

456 Methodology: MG, ZW, RJT

457 Project Administration: RJT, ZW

458 Supervision: ZW, RJT

459 Writing – Original Draft: MG

460 Writing – Review and Edits: MG, ZW, RJT

461

462 **Competing Interests:**

463 Authors declare they have no competing interest.

464

465 **Acknowledgements**

466 We acknowledge the NCAR Computation and Information Systems Laboratory (CISL) for

467 providing computing resources through Derecho. All ERA5 data are available used in this study

468 are available at the research data archive. Tornado report data is available through the NOAA

469 Storm Prediction Center severe weather database.

470

471

472 References

473 [Allen, J. T., Tippett, M. K., and Sobel, A. H.: Influence of the El Nino/Southern Oscillation on tornado and](#)
474 [hail frequency in the United States, *Nat. Geosci.*, 8, 278–283, <https://doi.org/10.1038/ngeo2385>, 2015.](#)

475 Ashley, W. S. and Strader, S. M.: Recipe for Disaster: How the Dynamic Ingredients of Risk and Exposure
476 Are Changing the Tornado Disaster Landscape, *Bull. Am. Meteorol. Soc.*, 97, 767–786,
477 <https://doi.org/10.1175/BAMS-D-15-00150.1>, 2016.

478 [Bieringer, P. and Ray, P. S.: A Comparison of Tornado Warning Lead Times with and without NEXRAD](#)
479 [Doppler Radar, *Weather Forecast.*, 11, 47–52, \[https://doi.org/10.1175/1520-\]\(https://doi.org/10.1175/1520-0434\(1996\)011<0047:ACOTWL>2.0.CO;2\)](#)
480 [0434\(1996\)011<0047:ACOTWL>2.0.CO;2, 1996.](#)

481 Brooks, H. E., Lee, J. W., and Craven, J. P.: The Spatial Distribution of Severe Thunderstorm and Tornado
482 Environments from Global Reanalysis Data, *Atmospheric Res.*, 67–68, 73–94,
483 [https://doi.org/10.1016/S0169-8095\(03\)00045-0](https://doi.org/10.1016/S0169-8095(03)00045-0), 2003.

484 Brooks, H. E., Carbin, G. W., and Marsh, P. T.: Increased Variability of Tornado Occurrence in the United
485 States, *Science*, 346, 349–352, <https://doi.org/10.1126/science.1257460>, 2014.

486 Charney, J. G. and DeVore, J. G.: Multiple Flow Equilibria in the Atmosphere and Blocking, *J. Atmospheric*
487 *Sci.*, 36, 1205–1216, [https://doi.org/10.1175/1520-0469\(1979\)036<1205:MFEITA>2.0.CO;2](https://doi.org/10.1175/1520-0469(1979)036<1205:MFEITA>2.0.CO;2), 1979.

488 [Cook, A. R., Leslie, L., Parsons, D., and Schaefer, J. T.: The ~~ImpactRelation~~ of El Nino-Southern Oscillation](#)
489 [\(ENSO\) ~~onto~~ Winter and Early Spring U.S. Tornado Outbreaks, *J. Appl. Meteorol. Climatol.*, 56, 2455–](#)
490 [2478 *Mon. Weather Rev.*, 136, 3121–3137, <https://doi.org/10.1175/JAMC-D-16-02492007MWR2171.1>,](#)
491 [2017 *2008*.](#)

492 Corti, S., Molteni, F., and Palmer, T. N.: Signature of Recent Climate Change in Frequencies of Natural
493 Atmospheric Circulation Regimes, *Nature*, 398, 799–802, <https://doi.org/10.1038/19745>, 1999.

494 Cwik, P., McPherson, R. A., Richman, M. B., and Mercer, A. E.: Climatology of 500-hPa Geopotential
495 Height Anomalies Associated with May Tornado Outbreaks in the United States., *Int. J. Climatol.*, 43,
496 893–913, <https://doi.org/10.1002/joc.7841>, 2022.

497 Del Genio, A. D., Yao, M.-S., and Jonas, J.: Will Moist Convection be Stronger in a Warmer Climate?,
498 *Geophys. Res. Lett.*, 34, <https://doi.org/10.1029/2007GL030525>, 2007.

499 Diffenbaugh, N. S., Scherer, M., and Trapp, R. J.: Robust Increases in Severe Thunderstorm Environments
500 in Response to Greenhouse Forcing, *Proc. Natl. Acad. Sci. U. S. A.*, 110, 16361–16366,
501 <https://doi.org/10.1073/pnas.1307758110>, 2013.

502 [Geng, T., Jia, F., Cai, W., Wu, L., Gan, B., Jing, Z., Li, S., and McPhaden, M. J.: Increased Occurrences of](#)
503 [Consecutive La Nina events under Global Warming, *Nature*, 619, 774–781,](#)
504 [https://doi.org/10.1038/s41586-023-06236-9, 2023.](#)

505 [Falkena, S. K. J., Wiljes, J. de, Weisheimer, A., and Shepherd, T. G.: Revisiting the identification of](#)
506 [wintertime atmospheric circulation regimes in the Euro-Atlantic sector, Q. J. R. Meteorol. Soc., 146,](#)
507 [2801–2814, <https://doi.org/10.1002/qj.3818>, 2020.](#)

508 Gensini, V. A. and Brooks, H. E.: Spatial Trends in United States Tornado Frequency, *Nature*, 1,
509 <https://doi.org/10.1038/s41612-018-0048-2>, 2018.

510 Graber, M., Trapp, R. J., and Wang, Z.: The Regionality and Seasonality of Tornado Trends in the United
511 States, *Npj Clim. Atmospheric Sci.*, 7, <https://doi.org/10.1038/s41612-024-00698-y>, 2024.

512 [Grams, C. M., Beerli, R., Pfenninger, S., Staffell, I., and Wernli, H.: Balancing Europe’s Wind-power](#)
513 [Output through spatial development informed by weather regimes, *Nat. Clim. Change*, 7, 557–562,](#)
514 [https://doi.org/10.1038/nclimate3338, 2017.](#)

515 [Grams, C. M., Ferranti, L., and Magnusson, L.: How to make use of weather regimes in Extended-range](#)
516 [Predictions for Europe, *ECMWF Newsl.*, 2020.](#)

517 Hannachi, A., Straus, D. M., Franzke, C. L. E., Corti, S., and Woollings, T.: Low-Frequency Nonlinearity and
518 Regime Behavior in the Northern Hemisphere Extratropical Atmosphere, *Rev. Geophys.*, 55, 199–234,
519 <https://doi.org/10.1002/2015RG000509>, 2017.

520 Hersbach, H., Bell, B., Berrisford, P., Hirahara, S., Horányi, A., Muñoz-Sabater, J., Nicolas, J., Peubey, C.,
521 Radu, R., Schepers, D., Simmons, A., Soci, C., Abdalla, S., Abellan, X., Balsamo, G., Bechtold, P., Biavati,
522 G., Bidlot, J., Bonavita, M., De Chiara, G., Dahlgren, P., Dee, D., Diamantakis, M., Dragani, R., Flemming,
523 J., Forbes, R., Fuentes, M., Geer, A., Haimberger, L., Healy, S., Hogan, R. J., Hólm, E., Janisková, M.,
524 Keeley, S., Laloyaux, P., Lopez, P., Lupu, C., Radnoti, G., de Rosnay, P., Rozum, I., Vamborg, F., Villaume,
525 S., and Thépaut, J.-N.: The ERA5 global reanalysis, *Q. J. R. Meteorol. Soc.*, 146, 1999–2049,
526 <https://doi.org/10.1002/qj.3803>, 2020.

527 Kodinariya, T. M. and Makwana, P. R.: Review on Determining Number of Clusters in K-Means
528 Clustering., *Int. J. Adv. Res. Comput. Sci. Manag. Stud.*, 1, 90–95, 2013.

529 Lee, S. H. and Messori, G.: The Dynamical Footprint of Year-Round North American Weather Regimes,
530 *Geophys. Res. Lett.*, 51, 2024.

531 [Lee, S.-K., Wittenberg, A. T., Enfield, D. B., Weaver, S. J., Wang, C., and Atlas, R.: US Regional Tornado](#)
532 [Outbreaks and their Links to Spring ENSO Phases and North Atlantic SST Variability, *Environ. Res. Lett.*,](#)
533 [11, <https://doi.org/10.1088/1748-9326/11/4/044008>, 2016.](#) [H., Tippett, M. K., and Polvani, L. M.: A New](#)
534 [Year-Round Weather Regime Classification for North America, *J. Clim.*, 36, 7091–7108,](#)
535 [https://doi.org/10.1175/JCLI-D-23-0214.1, 2023.](#)

536 Mercer, A. E. and Bates, A.: Meteorological Differences Characterizing Tornado Outbreak Forecasts of
537 Varying Quality, *Atmosphere*, 1, 16, <https://doi.org/10.3390/atmos10010016>, 2019.

538 Mercer, A. E., Shafer, C. M., Doswell III, C. A., Leslie, L. M., and Richman, M. B.: Synoptic Composites of
539 Tornadoic and Nontornadoic Outbreaks, *Mon. Weather Rev.*, 140, 2590–2608,
540 <https://doi.org/10.1175/MWR-D-12-00029.1>, 2012.

541 Michelangeli, P.-A., Vautard, R., and Legras, B.: Weather Regimes: Recurrence and Quasi Stationarity, J.
 542 Atmospheric Sci., 52, 1237–1256, [https://doi.org/10.1175/1520-](https://doi.org/10.1175/1520-0469(1995)052%3C1237:WRRAS%3E2.0.CO;2)
 543 0469(1995)052%3C1237:WRRAS%3E2.0.CO;2, 1995.

544 Miller, D., Wang, Z., Trapp, R. J., and Harnos, D. S.: Hybrid Prediction of Weekly Tornado Activity Out to
 545 Week 3: Utilizing Weather Regimes, Geophys. Res. Lett., 47, <https://doi.org/10.1029/2020GL087253>,
 546 2020.

547 Miller, D., Gensini, V. A., and Barrett, B. S.: Madden-Julian Oscillation Influences United States
 548 Springtime Tornado and Hail Frequency, Npj Clim. Atmospheric Sci., 5, [https://doi.org/10.1038/s41612-](https://doi.org/10.1038/s41612-022-00263-5)
 549 022-00263-5, 2022.

550 Moore, T. W.: Annual and Seasonal Tornado Trends in the Contiguous United States and its Regions, Int.
 551 J. Climatol., 38, 1582–1594, <https://doi.org/10.1002/joc.5285>, 2018.

552 Moore, T. W. and DeBoer, T. A.: A Review and Analysis of Possible Changes to the Climatology of
 553 Tornadoes in the United States, Prog. Phys. Geogr. Earth Environ., 43,
 554 <https://doi.org/10.1177/0309133319829398>, 2019.

555 NCEI: U.S. Billion-Dollar Weather and Climate Disasters, 2024.

556 Niloufar, N., Devineni, N., Were, V., and Khanbilvardi, R.: Explaining the Trends and Variability in the
 557 United States Tornado Records using Climate Teleconnections and Shifts in Observational Practices, Sci.
 558 Rep., 11, <https://doi.org/10.1038/s41598-021-81143-5>, 2021.

559 Rasmussen, E. N. and Blanchard, D. O.: A Baseline Climatology of Sounding-Serived Supercell and
 560 Tornado Forecast Parameters., Weather Forecast., 13, 1148–1164, [https://doi.org/10.1175/1520-](https://doi.org/10.1175/1520-0434(1998)013<1148:ABCOSD>2.0.CO;2)
 561 0434(1998)013<1148:ABCOSD>2.0.CO;2, 1998.

562 [Robertson, A. W. and Ghil, M.: Large-Scale Weather Regimes and Local Climate over the Western United](#)
 563 [States, J. Clim., 12, 1796–1813, https://doi.org/10.1175/1520-](#)
 564 [0442\(1999\)012%3C1796:LSWRAL%3E2.0.CO;2, 1999.](#)

565 [Robertson, A. W., Vignaud, N., Yuan, J., and Tippet, M. K.: Toward Identifying Subseasonal Forecasts of](#)
 566 [Opportunity Using North American Weather Regimes, Mon. Weather Rev., 148, 1861–1875,](#)
 567 [https://doi.org/10.1175/MWR-D-19-0285.1, 2020.](#)

568 Storm Prediction Center: U.S. Killer Tornado Statistics, 2024.

569 Strader, S. M., Ashley, W. S., Pingel, T. J., and Krmenc, A. J.: Projected 21st Century Changes in Tornado
 570 Exposure, Risk, and Disaster Potential, Clim. Change, 141, 301–313, [https://doi.org/10.1007/s10584-](https://doi.org/10.1007/s10584-017-1905-4)
 571 017-1905-4, 2017.

572 Strader, S. M., Gensini, V. A., Ashley, W. S., and Wagner, A. N.: Changes in Tornado risk and Societal
 573 Vulnerability Leading to Greater Tornado Impact Potential, Npj Nat. Hazards, 1, 2024.

574 Thompson, D. B. and Roundy, P. E.: The Relationship between the Madden-Julian Oscillation and US
 575 Violent Tornado Outbreaks in the Spring, Mon. Weather Rev., 141, 2087–2095,
 576 <https://doi.org/10.1175/MWR-D-12-00173.1>, 1998.

577 Thompson, R. L., Smith, B. T., Grams, J. S., Dean, A. R., and Broyles, C.: Convective Modes for Significant
 578 Severe Thunderstorms in the Contiguous United States. Part II: Supercell and QLCS Tornado
 579 Environments, *Weather Forecast.*, 27, 1136–1154, <https://doi.org/10.1175/WAF-D-11-00116.1>, 2012.

580 Tippett, M. K.: Changing Volatility of U.S. Annual Tornado Reports, *Geophys. Res. Lett.*, 41, 6956–6961,
 581 <https://doi.org/10.1002/2014GL061347>, 2014.

582 Tippett, M. K., Sobel, A. H., Camargo, S. J., and Allen, J. T.: An Empirical Relation between U.S. Tornado
 583 Activity and Monthly Environmental Parameters, *J. Clim.*, 27, 2983–2999, [https://doi.org/10.1175/JCLI-](https://doi.org/10.1175/JCLI-D-13-00345.1)
 584 [D-13-00345.1](https://doi.org/10.1175/JCLI-D-13-00345.1), 2014.

585 Tippett, M. K., Lepore, C., and L’Heureux, M. L.: Predictability of a Tornado Environment Index from El
 586 Nino Southern Oscillation (ENSO) and the Arctic Oscillation, *Weather Clim. Dyn.*, 3, 1063–1075,
 587 <https://doi.org/10.5194/wcd-3-1063-2022>, 2022.

588 Tippett, M. K., Malloy, K., and Lee, S. H.: Modulation of U.S. Tornado Activity by year-round North
 589 American Weather Regimes, *Mon. Weather Rev.*, <https://doi.org/10.1175/MWR-D-24-0016.1>, 2024.

590 Trapp, R. J.: *Mesoscale-Convective Processes in the Atmosphere*, Cambridge University Press, 2013.

591 Trapp, R. J.: On the Significance of Multiple Consecutive Days of Tornado Activity, *Mon. Weather Rev.*,
 592 142, 1452–1459, <https://doi.org/10.1175/MWR-D-13-00347.1>, 2014.

593 Trapp, R. J., Diffenbaugh, N. S., Brooks, H. E., Baldwin, M. E., Robinson, E. D., and Pal, J. S.: Changes in
 594 Severe Thunderstorm Environment Frequency during the 21st Century caused by Anthropogenically
 595 Enhanced Global Radiative Forcing, *Proc. Natl. Acad. Sci. U. S. A.*, 104, 19719–19723,
 596 <https://doi.org/10.1073/pnas.0705494104>, 2007.

597 Vigaud, N., Tippett, M. K., and Robertson, A. W.: Probabilistic Skill of Subseasonal Precipitation Forecasts
 598 for the East Africa-West Asia Sector during September-May, *Weather Forecast.*, 33, 1513–1532,
 599 <https://doi.org/10.1175/WAF-D-18-0074.1>, 2018.

600 Wakimoto, R. M. and Wilson, J. W.: Non-supercell Tornadoes, *Mon. Weather Rev.*, 117, 1113–1140,
 601 [https://doi.org/10.1175/1520-0493\(1989\)117<1113:NST>2.0.CO;2](https://doi.org/10.1175/1520-0493(1989)117<1113:NST>2.0.CO;2), 1989.

602